Bubble Formation in High-Pressure Liquid–Solid Suspensions with Plenum Pressure Fluctuation

G. Q. Yang, X. Luo, R. Lau, and L. S. Fan
Dept. of Chemical Engineering, The Ohio State University, Columbus, OH 43210

The behavior of bubble formation from a single orifice in a nonaqueous liquid and a liquid–solid suspension with pressure fluctuations in the gas chamber (plenum region) is studied at high pressures (up to 8.3 MPa). An analytical model is developed to account for the initial bubble size in liquid–solid suspensions at high pressures. The model takes into consideration various forces induced by particles, such as suspension inertial force. Both experiments and model predictions indicate that the initial bubble size in the suspension is generally larger than that in the liquid, and that it increases with an increase in the solids concentration. The system pressure has a significant effect on the initial bubble size in liquids or liquid–solid suspensions when bubbles are formed under variable gas flow-rate conditions, and a negligible effect under constant gas flow-rate conditions. This model can reasonably describe the initial bubble sizes under high-pressure conditions measured experimentally in this study and those reported in the literature.

Introduction

Bubble-column and slurry bubble-column reactors are widely used in industry, particularly in the chemical and petrochemical industries. Many industrial processes of considerable commercial interest are conducted under high pressures, such as methanol synthesis, resid hydrotreating, Fischer-Tropsch synthesis, and benzene hydrogenation. Studies in the literature have indicated significant effects of pressure on the hydrodynamics and transport phenomena in bubble columns and slurry bubble columns (Idogowa et al., 1986; Tarmy et al., 1984; Wilkinson, 1991; Inga, 1997; Luo et al., 1999). It is well known that elevated pressures lead to smaller bubble size and narrower bubble-size distribution. The bubble size in bubble columns is dictated by three processes: bubble formation, bubble coalescence, and bubble breakup. To fully understand the effect of pressure on the bubble size, it is necessary to examine the bubble-formation process in both liquids and liquid–solid suspensions under high-pressure conditions.

The phenomenon of bubble formation from a submerged single orifice connected to a gas chamber varies with gas injection conditions, which are characterized by the dimensionless capacitance number N_c defined as $4V_c g \rho_l/\pi D_0^2 P_s$ (Kumar and Kuloor, 1970; Tsuge and Hibino, 1983). When N_c is smaller than 1, the gas flow rate through the orifice is constant, which is characterized as constant flow conditions. When N_c is larger than 1, the gas flow rate through the orifice is not constant, and it is dependent on the pressure difference between the gas chamber and bubble. Such bubble-formation conditions are characterized as variable flow conditions in this study. In the literature, there have been experimental and theoretical studies on the effect of pressure or gas density on the initial bubble size from a single orifice submerged in liquids under constant flow conditions (Idogawa et al., 1987; Luo et al., 1998a) and variable flow conditions (LaNauze and Harris, 1974; Tsuge et al., 1992; Wilkinson and van Dierendonck, 1994; Yoo et al., 1998). The high-pressure studies indicate that an increase in gas density or system pressure reduces the size of bubbles formed from the orifice. The extent of the pressure effect on the initial bubble size depends on the bubble-formation conditions. Under constant flow conditions, the effect of pressure on the initial bubble size is insignificant (Luo et al., 1998a); however, under variable flow conditions, the pressure affects the initial bubble size significantly (Tsuge et al., 1992; Wilkinson and van Dierendonck, 1994).

Correspondence concerning this article should be addressed to L. S. Fan.

Although work on bubble formation in liquids at elevated pressures is available in the literature, little is known regarding the fundamental characteristics of bubble formation in liquids with the presence of solid particles. Yoo et al. (1997) investigated the bubble-formation process under variable flow conditions in a pressurized system with the presence of solid particles. In their experiments, glycerol aqueous solution and 0.1-mm polystyrene beads were used as the liquid and solid phases, respectively. The densities of the liquid and particles are the same; thus, the particles are neutrally buoyant in the liquid and do not induce particle inertial effect on the bubble. The results of Yoo et al.'s study indicated that the initial bubble size decreases significantly with increasing pressure. A homogeneous approach quantifying the particle effect is used in their bubble-formation model. Both their experimental results and model predictions indicated that the particle effect on the initial bubble size is insignificant, which is clearly due to the neutrally buoyant nature of particles used in their study.

Luo et al. (1998a) investigated the mechanism of single-bubble formation in a slurry system with a significant liquid and particle-density difference at pressures up to 17.3 MPa under constant-flow conditions. They found that bubbles formed from a single orifice in the liquid–solid suspension are larger than those formed in the liquid, and that the initial bubble size increases with increasing solids concentration. The bubble-formation model of Luo et al. (1998a) indicated that the particle effect on the bubble formation is mainly due to the inertia of the liquid–solid suspension and the collision between the bubble and particles. It was also found that the pressure effect is insignificant in liquid–solid suspensions under constant flow conditions, which is similar to the findings of Wilkinson and van Dierendonck (1994) obtained in liquids. The reason is that the effects of pressure on the overall upward forces and overall downward forces governing the bubble formation are comparable and the overall pressure effect is negligible under constant flow conditions. Further work is needed to quantify the effect of pressure on the initial bubble size under variable flow conditions in liquid–solid suspensions.

This study examines the effects of pressure and solids concentration on the phenomenon of bubble formation from a single orifice with pressure fluctuations in the gas chamber. Hydrocarbon liquid in the presence and absence of particles is used for the experiments. A mechanistic model is developed to account for the initial bubble size in the liquid-solid suspension under various bubble formation conditions. The mechanisms underlining the particle and pressure effects on bubble-formation behavior are discussed in light of the model.

Mathematical Model

A two-stage spherical bubble formation model (Ramakrishnan et al., 1969; Tsuge and Hibino, 1978; Luo et al., 1998a) is extended in this study to describe the bubble-formation process in liquids–solid suspensions with pressure fluctuations in the gas chamber. In the two-stage model, bubbles are assumed to be formed in two stages, namely, the expansion stage and the detachment stage. The bubble expands with its base attached to the orifice during the expansion stage. In the detachment stage, the bubble base moves away from the orifice and remains connected to the orifice through a neck. The shape of the bubble is assumed to remain spherical in the entire bubble-formation process. It is also assumed in this model that a liquid film always exists around the bubble. During the expansion and detachment stages, particles collide with the bubble and stay on the liquid film. The particles and the liquid surrounding the bubble are displaced and set in motion by the bubble as the bubble grows and rises. The bubble formation is shown in Figure 1.

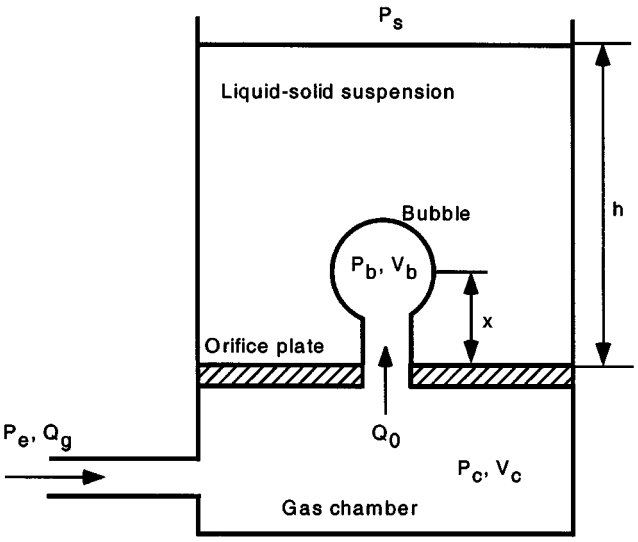

Figure 1. Bubble formation from a single orifice connected to a gas chamber.

Luo et al. (1998a) successfully extended the two-stage spherical bubble-formation model to simulate the bubble formation in liquid–solid suspensions under constant-flow conditions. In order to extend this model to simulate the bubble formation in liquid–solid suspensions under variable flow conditions, the particle effects on the bubble motion and the pressure balance at the bubble–liquid interface need to be considered. A detailed description of the model equations and modifications of the model are given in the following subsections.

Bubble motion equation

The motion equation of a rising bubble in liquid–solid suspensions can be described based on a balance of all the forces acting on the bubble (Luo et al., 1998a). The forces induced by the liquid include the upward forces [effective buoyancy (F_B) and gas momentum (F_M) forces], and the downward resistance [liquid drag (F_D), surface-tension force (F_σ), bubble inertial force ($F_{I,g}$), and Basset force (F_{Basset})]. Two other downward forces on the bubble account for the particle effect on the bubble motion, that is, the particle–bubble collision force (F_C) and the suspension inertial force ($F_{I,m}$) due to the acceleration of the liquid and particles surrounding the bubble (Luo et al., 1998a). Therefore, the overall force balance on the bubble formed in liquid–solid suspensions can be written as

$$F_B + F_M = F_D + F_\sigma + F_{\text{Basset}} + F_{I,g} + F_C + F_{I,m}. \quad (1)$$

The expansion and detachment stages follow the same force-balance equation (Eq. 1), although the expressions for the same force in two stages may be different. The expressions for all the forces under two stages are given in Table 1. The particle–bubble collision force is merely the rate of momentum change of particles colliding with the bubble surface. The suspension inertial force can be derived from the suspension flow field around an accelerating bubble. Luo et al. (1998a) quantified the flow field of the suspension around a two-dimensional bubble by using the particle image velocimetry (PIV) technique and obtained the expression for the suspension inertial force, $F_{I,m}$:

$$F_{I,m} = \frac{d(\iiint \rho_m u_m \delta V)}{dt} = \zeta \frac{d}{dt}\left[\rho_m \left(\frac{4}{3}\pi r_b^3\right) u_b\right], \quad (2)$$

where the apparent density of the suspension is defined as:

$$\rho_m = \epsilon_s \rho_s + \epsilon_l \rho_l. \quad (3)$$

For bubbles formed in liquid–solid suspensions, the coefficient ζ is equal to 3.86 (Luo et al., 1998a). When bubbles are formed in liquids, the coefficient ζ is equal to 11/16, corresponding to the added mass in inviscid liquid (Milne-Thomson, 1955; Davidson and Schuler, 1960a). Detailed descriptions of these forces are given ion Luo et al. (1998a).

In the expansion stage, the rise velocity of the bubble, u_b, is equal to the bubble expansion velocity, or

$$u_b = u_e = \frac{dr_b}{dt}, \quad (4)$$

and the gas flow rate through the orifice, Q_0, can be expressed by the following equation:

$$Q_0 = \frac{dV_b}{dt} = 4\pi r_b^2 \frac{dr_b}{dt}. \quad (5)$$

Substituting the expressions of various forces in Table 1 into Eq. 1 and considering Eqs. 4–5, the force balance at the end of the expansion stage can be written as

$$\frac{d}{dt}\left[(\rho_g + \zeta\rho_m)\left(\frac{4}{3}\pi r_b^3\right)\frac{dr_b}{dt}\right] = \frac{4\pi r_b^3}{3}(\rho_l - \rho_g)g + \frac{\rho_g Q_0^2}{1/4\,\pi D_0^2} - 6\pi\mu_l r_b \frac{dr_b}{dt} - \pi D_0 \sigma \cos\gamma - \frac{1}{4}\pi D_0^2 \rho_s \epsilon_s \left(\frac{dr_b}{dt}\right)^2. \quad (6)$$

The term on the lefthand side represents the inertial forces of the bubble and suspension. The five terms on the right-hand side represent the buoyancy, gas momentum, viscous, surface tension, and particle–bubble collision forces, respectively.

In the detachment stage, the rise velocity of the bubble is the sum of the expansion velocity (u_e) and the bubble base rising velocity (u):

$$u_b = u + u_e = \frac{dx}{dt}, \quad (7)$$

where x is the vertical distance between the bubble center and orifice plate. The gas flow rate through the orifice can be expressed by

$$Q_0 = \frac{d(V_b + V_{\text{neck}})}{dt} = \frac{d\left[\frac{4}{3}\pi r_b^3 + \frac{1}{4}\pi D_0^2 (x - r_b)\right]}{dt} = 4\pi r_b^2 \frac{dr_b}{dt} + \frac{1}{4}\pi D_0^2 \left(\frac{dx}{dt} - \frac{dr_b}{dt}\right). \quad (8)$$

Table 1. Expressions of the Forces Involved in the Bubble-Formation Process

Forces	Expansion Stage	Detachment Stage
F_B	$\frac{4\pi}{3} r_b^3 (\rho_l - \rho_g) g$	Same as expansion stage
F_M	$\frac{\pi}{4} D_0^2 \rho_g u_0^2$	Same as expansion stage
F_D	$C_D(\pi r_b^2)\frac{\rho_l u_b^2}{2}$ $\quad (C_D = 24/Re)$	Same as expansion stage
F_σ	$\pi D_0 \sigma \cos\gamma$	Same as expansion stage
$F_{I,g}$	$\frac{d}{dt}[\rho_g(\frac{4}{3}\pi r_b^3)u_b]$	Same as expansion stage
F_{Basset}	Not applicable	$12 r_b^2 \sqrt{\pi \rho_l \mu_l t}\,\frac{du}{dt}$
F_C	$\frac{\pi}{4} D_0^2 (1+e) \epsilon_s \rho_s u_e^2$	$\pi r_b^2 \epsilon_s \rho_s u^2$
$F_{I,m}$	$\frac{d(\iiint \rho_m u_m \delta V)}{dt} = \zeta \frac{d}{dt}\left[\rho_m \left(\frac{4}{3}\pi r_b^3\right) u_b\right]$	Same as expansion stage

Source: Luo et al., 1998a.

Then, the motion equation of a bubble in the detachment stage can be written as follows:

$$\frac{d}{dt}\left[(\rho_g+\zeta\rho_m)\left(\frac{4}{3}\pi r_b^3\right)\frac{dx}{dt}\right]=\frac{4\pi r_b^3}{4}(\rho_l-\rho_g)g+\frac{\rho_g Q_0^2}{\frac{1}{4}\pi D_0^2}$$
$$-6\pi\mu_l r_b\frac{dx}{dt}-\pi D_0\sigma\cos\gamma-\pi r_b^2\rho_s\epsilon_s\left(\frac{d(x-r_b)}{dt}\right)^2$$
$$-12r_b^2\sqrt{\pi\rho_l\mu_l t}\,\frac{d^2(x-r_b)}{dt^2}. \quad (9)$$

The terms on the righthand side represent the buoyancy, gas momentum, viscous, surface tension, particle–bubble collision and Basset forces, respectively.

Orifice equation

The instantaneous gas flow rate through the orifice depends on the pressure difference between the gas chamber and bubble, and the orifice resistance. The following orifice equation is applicable (Kupferberg and Jameson, 1969):

$$|P_c-P_b|=\left(\frac{Q_0}{k_0}\right)^2, \quad (10)$$

where Q_0 is related to the rate of bubble volume change and can be calculated by using Eqs. 5 and 8 for the expansion and detachment stages, respectively. The orifice constant, k_0, is a function of gas flow rate Q_0, gas density ρ_g, gas viscosity μ_g, orifice diameter D_0, and orifice plate thickness L. Considering the pressure drop due to the sudden enlargement and contraction at the orifice and the frictional head loss, the following equation can be used to calculate k_0 (McAllister et al., 1958):

$$k_0=\sqrt{\frac{2}{\rho_g C_g}}\left(\frac{\pi D_0^2}{4}\right), \quad (11)$$

where

$$C_g=1.5+4f\frac{L}{D_0}. \quad (12)$$

Assuming that the flow of gas through the orifice is laminar, the friction factor, f, can be expressed by

$$f=\frac{16}{Re_0}=\frac{4\pi\mu_g D_0}{\rho_g Q_0}, \quad (13)$$

and substituting Eq. 13 into Eq. 12, the constant C_g can be estimated by the following equation:

$$C_g=1.5+\frac{16\pi\mu_g L}{\rho_g Q_0}. \quad (14)$$

Therefore, the pressure difference between the bubble and gas chamber can be calculated based on Eqs. 10, 11 and 14 if the gas flow rate through the orifice, properties of gas phase, and orifice geometry are known.

Pressure balance at bubble–liquid interface

The pressure inside the bubble can be obtained by considering the pressure balance at the bubble–liquid interface. The change of pressure along the bubble–liquid interface is mainly due to the inertia (ΔP_I), surface tension (ΔP_σ), and viscosity (ΔP_μ) of the liquid, and the gas momentum (ΔP_m), which can be expressed by the modified Rayleigh equation (Pinczewski, 1981):

$$P_b-P_0=\Delta P_I+\Delta P_\mu+\Delta P_\sigma-\Delta P_m. \quad (15)$$

The average hydrostatic pressure at the bubble surface, P_0, is approximately expressed by the hydrostatic pressure at the orifice plate as

$$P_0=P_s+\rho_l gh, \quad (16)$$

where P_s is the system pressure and h is the liquid level in the column. The four terms on the righthand side of Eq. 15 represent the contributions of liquid inertial, viscous, surface tension, and gas-momentum forces, respectively.

For inviscid liquids, the inertial term in Eq. 15 has been expressed in the literature based on the velocity potential around an expanding, rising bubble by (Kotake, 1966; Witze et al., 1968; Kupferberg and Jameson, 1969; McCann and Prince, 1969; Haynes and Gotham, 1982):

$$\Delta P_I=\rho_l\left(r_b\frac{d^2r_b}{dt^2}+\frac{3}{2}\left(\frac{dr_b}{dt}\right)^2-gx-\frac{1}{4}\left(\frac{dx}{dt}\right)^2\right). \quad (17)$$

However, Eq. 17 is valid only for ideal liquids. For highly viscous liquids or liquid–solid suspensions, the flow field around the bubble is different from that for inviscid liquids, which accounts for the difference in the inertial term. Davidson and Schuler (1960a,b) conducted a systematic study of the mechanism of bubble formation, and they derived 11/16 as an average value of the added mass coefficient for a bubble forming in an inviscid liquid. Marmur and Rubin (1976) used a similar concept and the velocity of the interface to define the inertia of the interface. They found that the added mass coefficient for the bubble-formation process in a viscous liquid higher than 11/16, the theoretical value for bubble formation in an inviscid liquid. In their study, they found that the value of the ''added mass'' coefficient is 0.85, which agrees well with their experimental results. Luo et al. (1998a) used the PIV technique to measure the flow field of the liquid–solid suspensions around an accelerating bubble. They found that the flow field in liquid–solid suspensions is quite different from that in liquids, resulting in an increase in iner-

tia. Therefore, in order to use Eq. 15 to simulate the bubble formation in liquid–solid suspensions, the effect of particles on the inertial term must be considered. The pressure change due to the suspension inertia can be expressed by

$$\Delta P_I = \frac{F_{I,m}}{A_b}, \tag{18}$$

where A_b is the surface area of the bubble, and $F_{I,m}$ is the suspension inertial force expressed by Eq. 2. Substituting Eq. 2 into Eq. 18, and considering the different expressions of the bubble velocity in the two stages, the inertial term in Eq. 15 can be modified to

$$\Delta P_I = \zeta \rho_m \left[\frac{r_b}{3} \frac{d^2 r_b}{dt^2} + \left(\frac{dr_b}{dt} \right)^2 \right] \quad \text{(expansion stage)} \tag{19a}$$

$$\Delta P_I = \zeta \rho_m \left[\frac{r_b}{3} \frac{d^2 x}{dt^2} + \frac{dr_b}{dt} \frac{dx}{dt} \right] \quad \text{(detachment stage)}. \tag{19b}$$

For a real liquid, it is difficult to theoretically obtain a precise expression of the pressure change across the bubble–liquid interface. The common approach used is to include the terms accounting for the effects of the viscosity, surface tension, and gas momentum on the pressure change in the Rayleigh equation, as shown in Eq. 15. Poritsky (1952) and Miyahara and Takahashi (1984) considered the effect of viscosity from the stress conditions on the bubble surface and derived the expression for the viscous term in the modified Rayleigh equation:

$$\Delta P_\mu = \frac{4\mu_l}{r_b} \frac{dr_b}{dt}. \tag{20}$$

The change of pressure along the bubble–liquid interface due to the surface tension can be given by (Levich, 1962):

$$\Delta P_\sigma = \frac{2\sigma}{r_b}. \tag{21}$$

Pinczewski (1981) derived an expression for the pressure distribution at the interface due to the gas momentum by assuming that the gas inside the growing bubble follows a circulatory toroidal motion:

$$\Delta P_{m,\theta} = \frac{1}{2} \rho_g u_0^2 \cos\theta, \tag{22}$$

where θ is the angle between the radial and vertical directions at any position of the bubble–liquid interface. Integrating Eq. 22 along the bubble surface, the average pressure change due to the gas momentum can be obtained:

$$\Delta P_m = \frac{\int_0^{2\pi} \Delta P_{m,\theta} \, d\theta}{2\pi} = \frac{1}{4} \rho_g u_0^2. \tag{23}$$

Substituting Eqs. 19–21 and 23 into Eq. 15, the modified Rayleigh equation can be extended for bubble formation in liquid–solid suspensions.

For the expansion stage:

$$P_b - P_0 = \zeta \rho_m \left[\frac{r_b}{3} \frac{d^2 r_b}{dt^2} + \left(\frac{dr_b}{dt} \right)^2 \right] + \frac{2\sigma}{r_b} + \frac{4\mu_l}{r_b} \frac{dr_b}{dt} - \frac{1}{4} \rho_g \left(\frac{Q_0}{\frac{1}{4}\pi D_0^2} \right)^2. \tag{24a}$$

For the detachment stage:

$$P_b - P_0 = \zeta \rho_m \left[\frac{r_b}{3} \frac{d^2 x}{dt^2} + \frac{dr_b}{dt} \frac{dx}{dt} \right] + \frac{2\sigma}{r_b} + \frac{4\mu_l}{r_b} \frac{dr_b}{dt} - \frac{1}{4} \rho_g \left(\frac{Q_0}{\frac{1}{4}\pi D_0^2} \right)^2. \tag{24b}$$

The instantaneous gas flow rate through the orifice, Q_0, can be calculated by using Eqs. 5 and 8 for the expansion and detachment stages, respectively. Equation 24 expresses the change of pressure inside the bubble during the bubble-formation process in liquid–solid suspensions.

Pressure change in the gas chamber

The change of pressure in the gas chamber, P_c, during the expansion and detachment stages is obtained by assuming an adiabatic or isothermal expansion process of ideal gas and applying the first law of thermodynamics to the gas in the chamber (Wilkinson and van Dierendonck, 1994):

$$\frac{dP_c}{dt} = \frac{\gamma}{V_c} \left(P_e Q_g - P_c Q_0 \right), \tag{25}$$

where P_e is the pressure at the gas inlet to the chamber. For the adiabatic change, γ is the specific heat ratio of the gas ($\gamma = C_p/C_v$); for the isothermal change, γ is equal to 1.

The radius of the bubble at the end of the expansion stage can be obtained by solving Eqs. 10, 24a, and 25 simultaneously under the following initial conditions:

$$t = 0, \quad r_b = \frac{1}{2} D_0, \frac{dr_b}{dt} = 0, \quad P_c = P_s + \rho_m g h + \frac{4\sigma}{D_0}. \tag{26}$$

It is assumed that the bubble is initially a hemisphere having a radius equivalent to the orifice radius. The termination of the expansion stage occurs at the time when various forces are in balance, as given by Eq. 6. The governing equations for the detachment stage, Eqs. 9, 10, 24b, and 25, can be solved by using the final values of the expansion stage as their initial

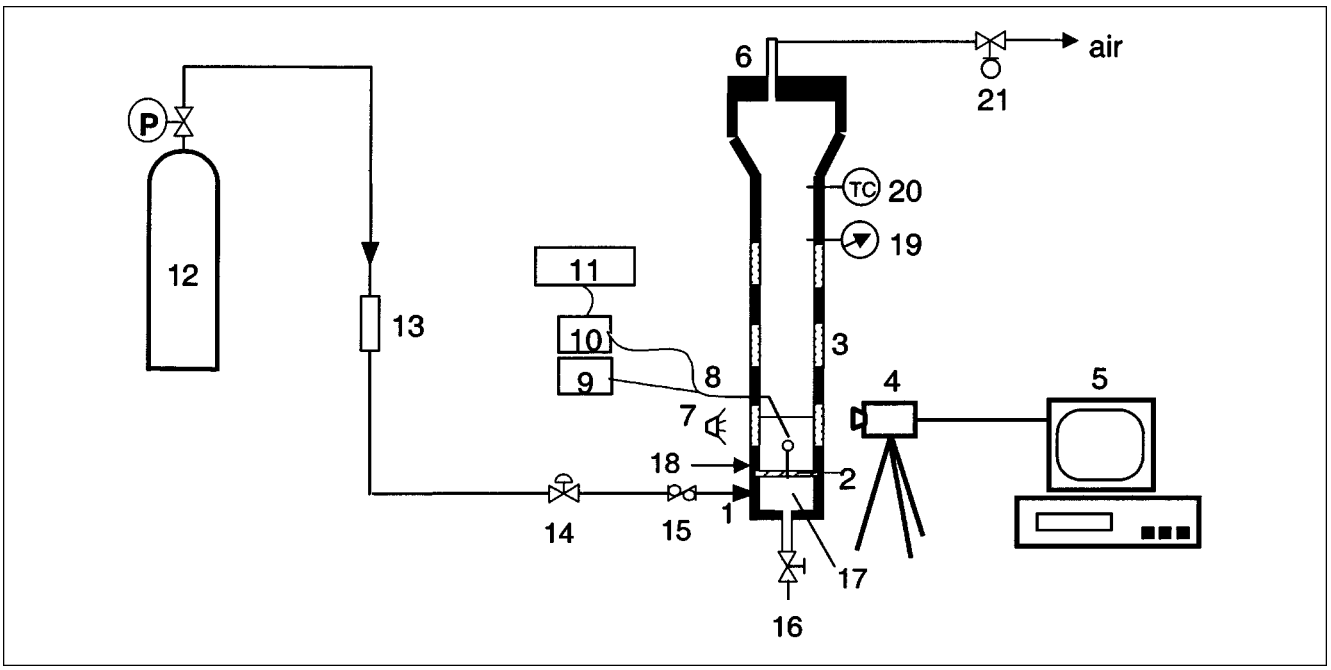

Figure 2. Experimental setup for the measurement of initial bubble size in high-pressure liquid–solid suspensions.

(1) Gas inlet; (2) distributor; (3) quartz windows; (4) high-speed video camera; (5) monitor and high-speed VCR; (6) gas outlet; (7) lighting; (8) fiber-optic probe; (9) light source; (10) photomultiplier; (11) data-acquisition system; (12) nitrogen cylinder; (13) mass flow meter; (14) needle valve; (15) check valve; (16) drain valve; (17) gas chamber; (18) auxiliary gas inlet; (19) pressure gauge; (20) thermocouple; (21) back pressure regulator.

conditions:

$$t = t_e, \quad r_b = r_e, \quad \frac{dr_b}{dt} = \left.\frac{dr_b}{dt}\right|_{t=t_e}, \quad x = r_e, \frac{dx}{dt} = \left.\frac{dr_b}{dt}\right|_{t=t_e}, \quad P_c = P_{c,e}, \quad (27)$$

where subscript e represents the end of the expansion stage. When the neck length reaches r_e, that is, $x - r_b = r_e$, the bubble detaches from the orifice and the calculation is terminated (Ramakrishnan et al., 1969). The bubble volume at this instant gives rise to the final size of the bubble. The governing equations for both stages are coupled ordinary differential equations and can be solved simultaneously by using the fourth-order Runge-Kutta method.

Experimental Studies

The high-pressure three-phase fluidized bed used in this work for measuring the initial bubble size in liquid–solid suspensions is shown in Figure 2. The fluidized bed is a stainless-steel column 1.38 m in height at 0.102 m ID, consisting of three sections: the plenum, test, and disengagement sections. The column can be operated at pressures up to 21 MPa and temperatures up to 180°C. Three pairs of quartz windows are installed on the front and rear sides of the column. Each window is 12.7 mm wide and 93 mm long. The system pressure is adjusted and controlled by the back pressure regulator located at the column exit. A pressure gauge installed in the test section is used to monitor the pressure change in the column.

Nitrogen from a compressed cylinder (6,000 psig, 41 MPa) is injected into the liquid–solid medium through a single orifice of 1.63 mm in diameter and 3 mm in thickness. The orifice is attached to a stainless-steel gas chamber with a volume of 650 cm^3 through a 3/8-in. (9.5-mm) tube. The tube length is 0.12 m and the tube volume should be considered in the model calculations. The flow rate of nitrogen is controlled by adjusting a metering valve and measured by a mass flowmeter. The liquid phase is in batch operation. The particles are suspended by the auxiliary gas, which enters the column through a ring distributor surrounding the tube. After the particles are fully suspended, the auxiliary gas is shut off and

Table 2. Physical Properties of the Gas and Liquid Phases at Various Pressures

System pressure (MPa)	0.1	0.3	0.7	2.5	4.9	8.3
Gas density (kg/m^3)	1.1	3.3	7.8	27.8	54.5	92.2
Liquid density (kg/m^3)	867.8	868.1	868.6	871.2	874.6	879.4
Liquid viscosity (Pa·s)	0.0234	0.0237	0.0243	0.0270	0.0301	0.0337
Surface tension (N/m)	0.0292	0.0290	0.0286	0.0271	0.0258	0.0250

Note: $T = 30°C$

the measurement is conducted before the particles start to settle down. The height of the suspension is maintained at 0.4 m from the distributor.

In this study, the liquid phase is Paratherm NF heat transfer fluid. The physical properties of the gas and liquid phases vary with pressure. To fully understand the pressure effect on the initial bubble size, the variations of these properties need to be taken into account in the model. Table 2 shows the physical properties of the gas and liquid at various operating pressures. It is noted in the table that among various liquid properties, the liquid viscosity is the one most influenced by the system pressure. When the pressure increases from ambient pressure to 8.3 MPa, the liquid viscosity increases from 23.4 cp to 33.7 cp, or a 44% increase, compared to the 1.3% increase for the liquid density and the 14% decrease for the surface tension. The particles used in this study are glass beads of 210-μm diameter and 2,450 kg/m^3 density. In this study, the system pressure and solids concentration vary in the ranges of 0.1 to 8.3 MPa and 0 to 30 vol. %, respectively. The orifice gas velocity varies up to the jetting regime.

A fiber-optic probe (3 mm in OD) is used for detecting bubbles. The probe utilizes the difference in refractive indexes between the gas and liquid phases to distinguish the gas phase from the liquid or liquid–solid suspension. The frequency of bubble formation can be obtained through Fourier analysis of the light-intensity signals obtained from the probe. The details of the probe are given elsewhere (Luo et al., 1998b). In order to verify the validity of this measuring technique, a high-speed video camera (240 frames/s) is used to capture the images of bubbles emerging from the orifice in liquids, and the bubbling frequency is obtained by counting the number of bubbles during a fixed time interval. It is found that the bubble frequencies measured by these two techniques are almost identical. By assuming that the bubbles are of the same size, the volume of a single bubble can be calculated by dividing the gas flow rate entering the chamber by the measured bubbling frequency.

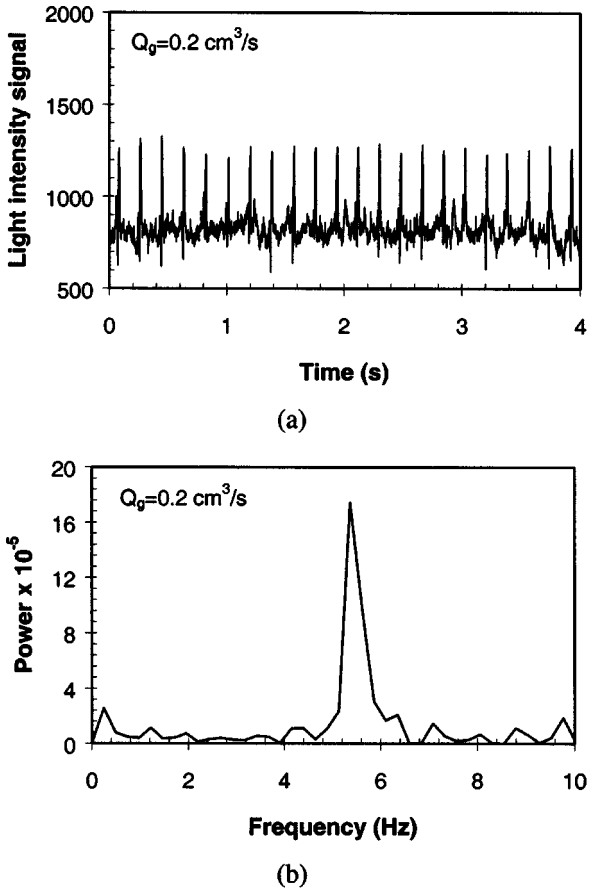

Figure 3. (a) Typical signal from the fiber-optic probe; (b) corresponding power spectrum in a pressurized slurry system.

$P_s = 2.5$ MPa; $\epsilon_s = 0.18$; $Q_g = 0.2$ cm^3/s.

Results and Discussion

Bubbling frequency

A typical signal of the light intensity obtained from the fiber-optic probe in a pressurized slurry bubble column is shown in Figure 3a. The discrete peaks in the time domain indicate the passage of bubbles over the probe. The power spectrum of the signal obtained by the Fourier analysis is shown in Figure 3b. As can be seen from the figure, the dominant frequency in the frequency domain corresponds to the frequency of bubble formation. Figure 4 shows the effect of pressure on the frequency of bubble formation in the liquid–solid suspension. As shown in the figure, the bubbling frequency increases with increasing orifice gas velocity, and elevated pressures lead to higher bubbling frequency. The pressure effect is more significant in the pressure range of 0.1 MPa to 2.5 MPa, in which the bubble formation is under variable flow conditions ($N_c > 1$). When the pressure is further increased, the bubble formation is under constant flow conditions ($N_c \leq 1$), and the change of bubbling frequency with pressure is not significant.

Initial bubble size and simulation results

Pressure Effect. A sequence of bubble images showing the process of bubble formation in liquids at the elevated pres-

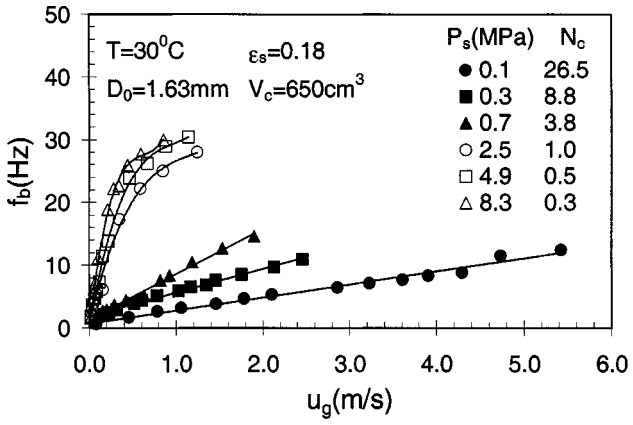

Figure 4. Effect of pressure on the frequency of bubble formation from a single orifice in the liquid–solid suspension.

$T = 30$°C; $D_0 = 1.63$ mm; $V_c = 650$ cm^3; $\epsilon_s = 0.18$.

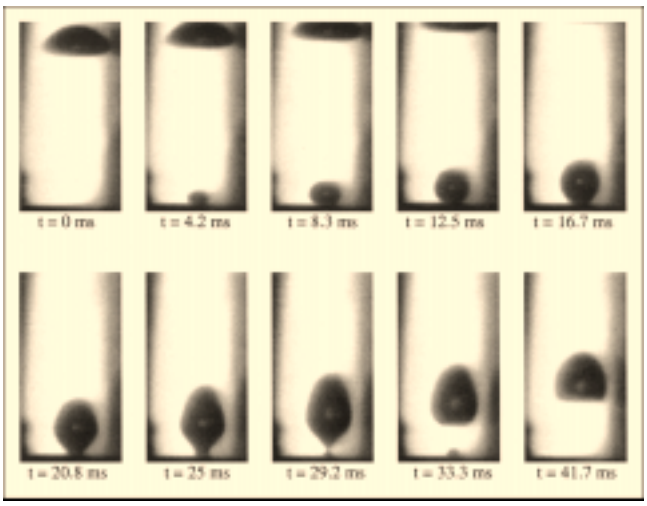

Figure 5. A sequence of bubble images showing the process of bubble formation in liquids at elevated pressures.

$P_s = 0.7$ MPa; $Q_g = 1.6$ cm^3/s.

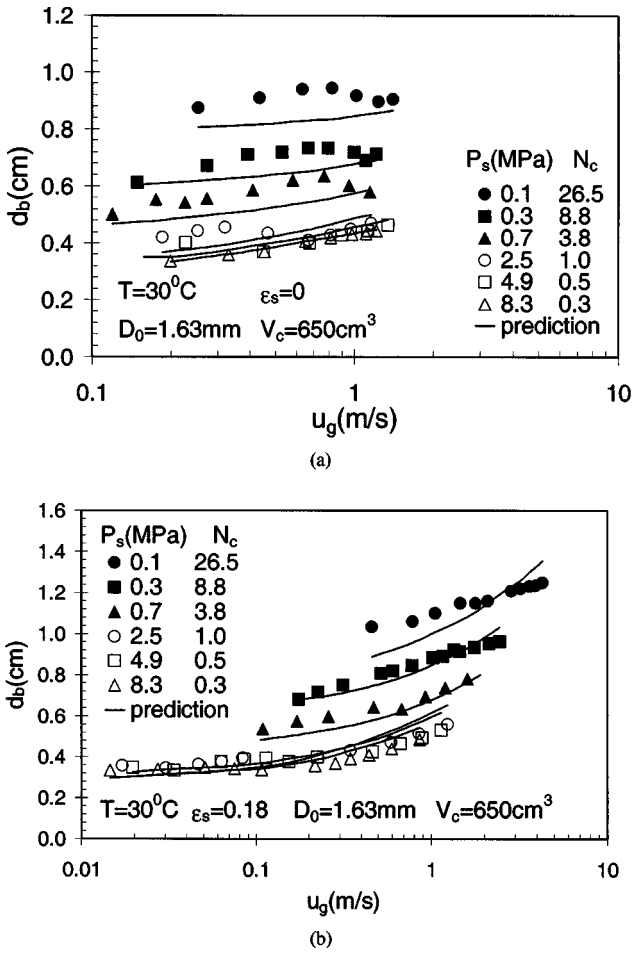

Figure 6. Effect of pressure on the initial bubble size.

$T = 30$°C; $D_0 = 1.63$ mm; $V_c = 650$ cm^3. (a) In the liquid ($\epsilon_s = 0$); (b) in the liquid–solid suspension ($\epsilon_s = 0.18$) (symbols, experimental data; lines, model predictions).

sure is shown in Figure 5. It can be seen that a bubble growing at the orifice remains roughly spherical until it detaches from the orifice. The two stages in the bubble-formation process, that is, the expansion stage and the detachment stage, can be seen clearly in Figure 5. Thus, the two-stage spherical model is justifiable for use in the simulation of the bubble-formation process in the present study. Figure 6 shows the experimental data and model predictions of the initial bubble size in the liquid and liquid–solid suspension under various pressures. It is found that the pressure effect on the initial bubble size depends strongly on the bubble-formation conditions. Under variable flow conditions ($N_c > 1$), an increase in pressure significantly reduces the initial bubble size in both the liquid and the liquid–solid suspension. For bubble formation under constant flow conditions ($N_c \leq 1$), the pressure effect is not significant, which is consistent with the findings of Wilkinson and van Dierendonck (1994), Yoo et al. (1997), and Luo et al. (1998a) for bubble formation in the liquid. For example, at the orifice gas velocity of 1.0 m/s and solids concentration of 18 vol. %, the initial bubble size decreases from 1.09 cm to 0.76 cm (30% decrease) when the pressure increases from 0.1 MPa to 0.7 MPa; however, at the same gas velocity and solids concentration, the initial bubble size only changes from 0.53 cm to 0.51 cm (4% decrease) when the pressure increases from 2.5 MPa to 8.3 MPa. The solid lines in Figure 6 represent the model predictions. It is found that the proposed model can reasonably predict the experimental results obtained in this study.

Generally, the initial bubble size is determined by the total bubble growth time and bubble growth rate, that is, the instantaneous gas flow rate entering the bubble Q_0. In order to analyze the pressure effect on the initial bubble size under various formation conditions, it is necessary to examine the pressure effects on the bubble-formation time and the gas flow rate entering the bubble. The bubble-formation time and instantaneous gas flow rate through the orifice can be estimated by the proposed model. The effect of pressure on the bubble-formation time in a slurry ($\epsilon_s = 0.18$) is shown in Figure 7. For bubble formation under variable flow conditions, the bubble-formation time slightly increases with increasing gas velocity and decreases significantly with increasing system pressure; while under constant flow conditions, the bubble-formation time only slightly changes with increasing gas velocity and system pressure. Figure 8 shows the change of the gas flow rate through the orifice with the time during the bubble-formation process. It is seen that at ambient or low pressures, the gas flow rate through the orifice, Q_0, varies significantly with time. At the beginning period of bubble growth, Q_0 increases rapidly to a maximum, which could be several times higher than the gas flow rate entering the chamber, Q_g. Then, Q_0 decreases gradually and approaches a constant value, which is close to Q_g. At high pressures, Q_0 increases first to a level slightly higher than Q_g; it then decreases and quickly reaches a constant flow rate, indicating that the bubble formation is under constant flow conditions. Commonly, when N_c is smaller than one, the bubble formation is considered to be under constant-flow conditions; however, from Figure 8 it is seen that even under such conditions, the fluctuation of gas flow rate still exists at the begin-

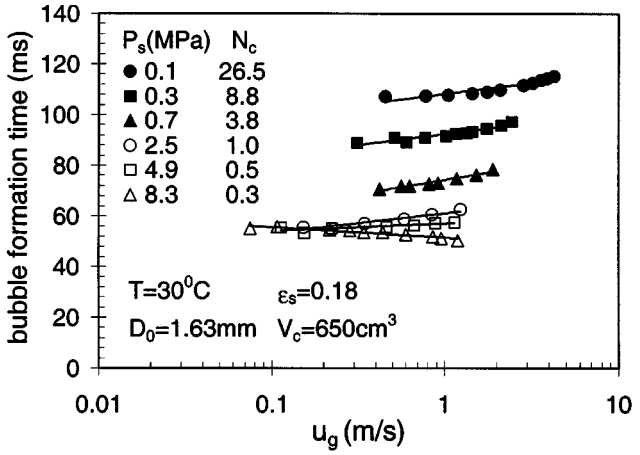

Figure 7. Bubble-formation time as a function of gas velocity at various pressure in the liquid–solid suspension.

$\epsilon_s = 0.18$.

ning of bubble growth, due to the existence of a large gas chamber underneath the orifice. It is also shown in Figure 8 that the curve of Q_0 vs. time shifts to the left when the pressure increases. This indicates that the bubble starts growing earlier under high pressures. Based on the preceding analysis, for bubble formation under variable flow conditions, the reductions of both the bubble-formation time and the gas rate through the orifice with increasing pressure result in the significant decrease of the initial bubble size.

The effect of pressure on bubble formation under variable flow conditions can be explained based on the proposed model. From the model, it can be seen that the pressure can influence the bubble-formation process through the following relationships: (1) the pressure directly influences the pressure fluctuation in the gas chamber based on the thermodynamic equation; (2) the pressure affects the gas momentum terms in the bubble motion equation and modified Rayleigh's equation through the change of gas density; (3) based on the orifice equation, the pressure can also influence the orifice resistance through the change of gas density, and hence the gas flow rate through the orifice. The model calculation shows that the pressure effect on the orifice constant mainly changes the gas flow rate entering the bubble. With increasing system pressure, the orifice constant becomes smaller due to the increase in gas density, and hence a decrease in the gas flow rate through the orifice. The bubble-formation time is determined by the force balance on the bubble and the pressure change in the gas chamber. The increase in pressure results in a higher gas momentum rate and larger pressure fluctuation in the gas chamber, which promote the detachment of the bubble and hence decrease the bubble-formation time. The combination of the preceding effects results in the decrease in the bubble-formation time and Q_0 with increasing pressure, and hence the decrease of the initial bubble size.

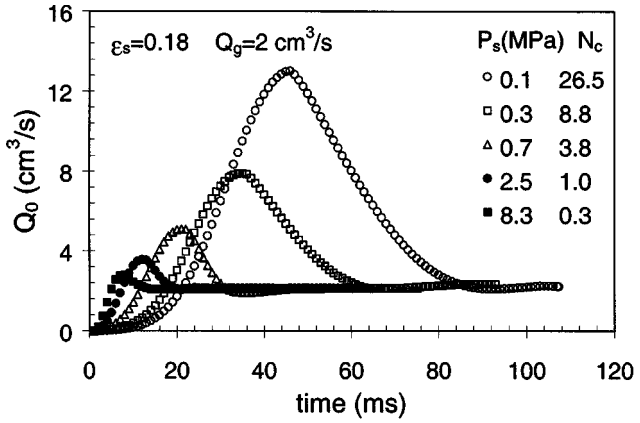

Figure 8. Effect of pressure on the variation of gas flow rate through the orifice with the time during the bubble-formation process in the liquid–solid suspension.

$\epsilon_s = 0.18$; $Q_g = 2$ cm^3/s.

Under constant flow conditions, the constant gas flow rate through the orifice and the weak dependence of the bubble formation time on the pressure, as shown in Figure 7, contribute to an insignificant effect of pressure on the initial bubble size. When the bubble is formed under constant flow conditions, the influence of pressure on the bubble-formation process is only caused through the gas momentum, as illustrated by the bubble motion equation. At low gas velocities, the influence of gas momentum is negligible, provided the pressure or gas density is low, resulting in an insignificant change of bubble formation time with the pressure, as shown in Figure 7. When the gas velocity is high, the influence of gas momentum becomes remarkable. The bubble tends to detach from the orifice earlier due to the increased gas momentum with the increase of gas density, which results in the reduction of bubble-formation time with increasing pressure and gas velocity.

Particle Effect. Figure 9 shows the particle effect on the initial bubble size under various bubble-formation conditions. For bubble formation under both constant flow and variable flow conditions, the bubbles formed in the liquid–solid suspension are larger in size than those formed in the liquid at a given gas velocity for the present system. For bubble formation in the liquid–solid suspension, a further increase in the solids concentrations only slightly increases the bubble size. The proposed model can also predict the trend of the particle effect. Based on the model calculations, the presence of particles in the liquid mainly influences the bubble growth time due to various forces induced by the particles on the bubble surface, such as suspension inertial force. The particles yield resistant forces for the detachment of bubbles, resulting in longer bubble formation time and hence larger bubble size.

Based on the model calculation, the comparison of the magnitude of various forces acting on the bubble at the end of the bubble-formation process in a slurry system is shown in Figure 10a. As shown in the figure, the suspension inertial force is the dominant downward force and the buoyancy force is the major upward force. At low pressures, the effect of gas momentum on the bubble formation is negligible; however, at high pressures, the gas-momentum force could play an important role in providing an upward force. It is noted that the Basset force is also important in dictating the bubble-formation process, especially at low pressures due to the large bub-

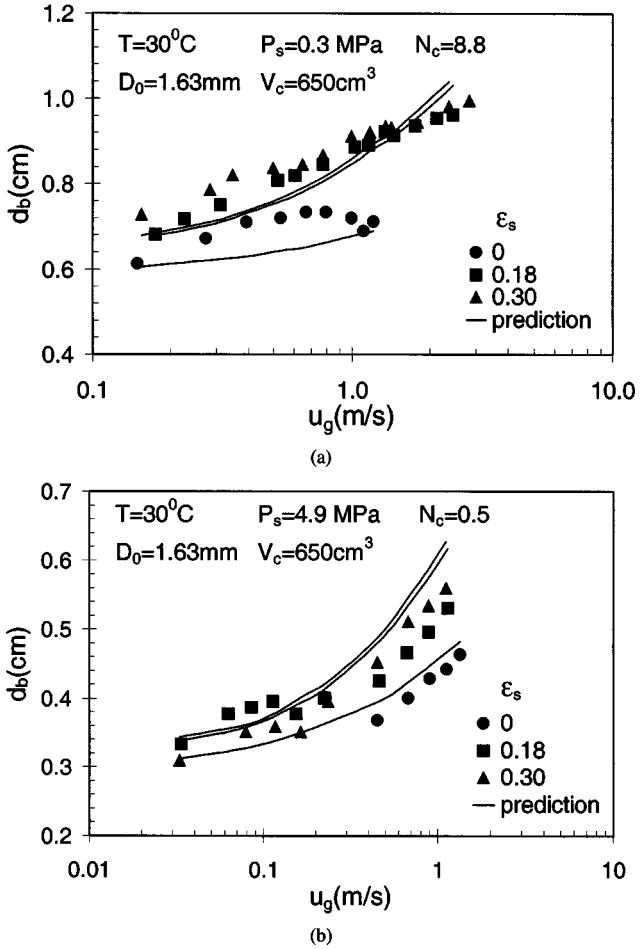

Figure 9. Effect of solids concentration on the initial bubble size.

$T = 30°C$; $D_0 = 1.63$ mm; $V_c = 650$ cm^3. (a) Variable flow conditions ($P_s = 0.3$ MPa; $N_c = 8.8$); (b) constant flow conditions ($P_s = 4.0$ MPa; $N_c = 0.5$) (symbols, experimental data; lines, model predictions).

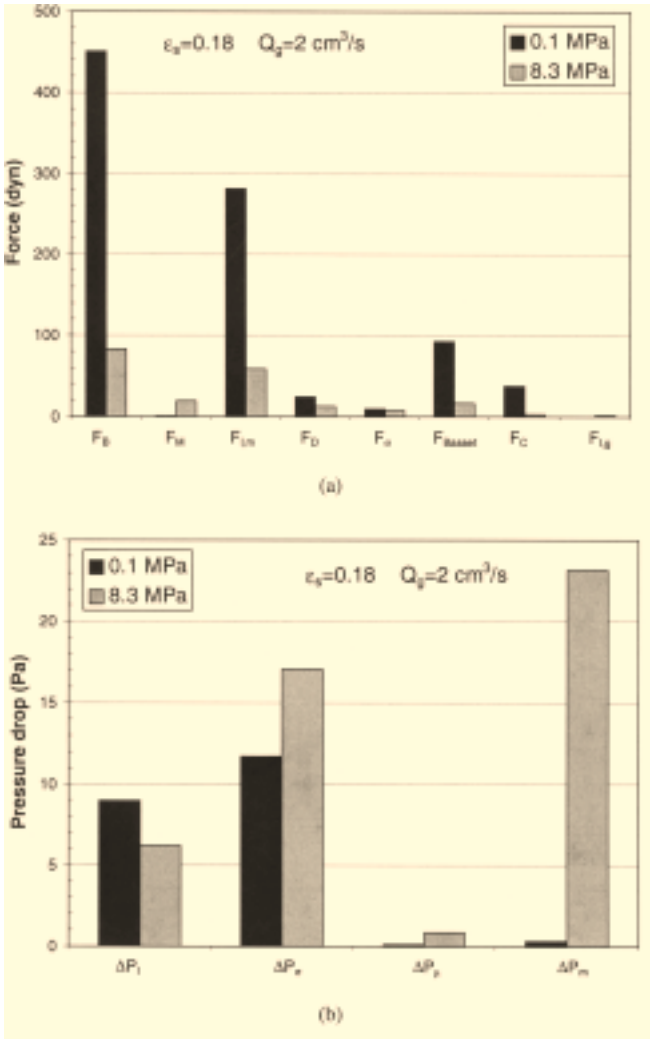

Figure 10. Contributions of various terms in: (a) bubble-motion equation; (b) pressure-balance equation for the bubble formation in the liquid–solid suspension.

$\epsilon_s = 0.18$; $Q_g = 2$ cm^3/s.

ble size. When the pressure increases, both the buoyancy and suspension inertial forces decrease significantly due to reduced bubble size.

The comparison of the contributions of various terms in the modified Rayleigh equation (Eq. 15) on the pressure drop across the bubble–liquid interface at the end of the bubble-formation process is shown in Figure 10b. It is found that the contributions of suspension inertia and surface tension are important at all pressures and the contribution of the viscous term is not significant. At high pressures, the contribution of gas momentum becomes dominant.

Prediction of Literature Data. To examine the applicability of the proposed model, the model is used to predict the available experimental data on bubble formation under high-pressure or high gas density conditions that are found in the literature. Figure 11 shows the comparison between the model predictions and the experimental literature data. It is found that the proposed model can reasonably predict these data. The average relative error of the predictions is 11%, and the confidence interval for the average error at the 95% confidence level is 10 to 12%. The relevant information on the various references used in Figure 11 is summarized in Table 3.

Bubble growth and pressure fluctuation in the gas chamber

The variations of the bubble volume and the pressure in the gas chamber with time simulated by the model are plotted in Figure 12. The effect of pressure on the bubble growth curve is shown in Figure 12a. In the pressure range of 0.1 MPa to 2.5 MPa, bubble formation is under variable-flow conditions and the bubble growth rate varies during the formation process. At the end of bubble formation, the bubble growth rate approaches a constant value. Under such conditions, with an increase in pressure, the bubble growth rate becomes smaller and the bubble growth time becomes shorter. When the pressure is higher than 2.5 MPa, the bubble growth

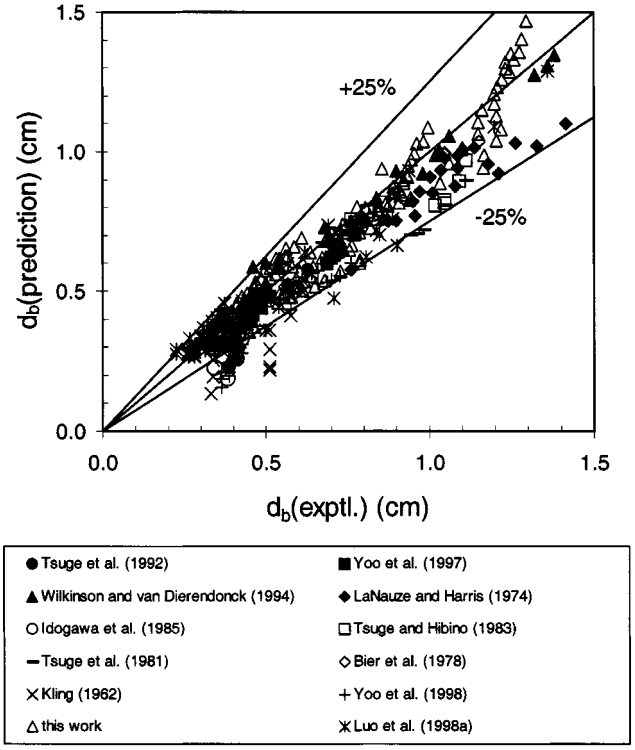

Figure 11. Model predictions vs. literature data of the initial bubble size under high-pressure conditions.

For information about literature data, see Table 3.

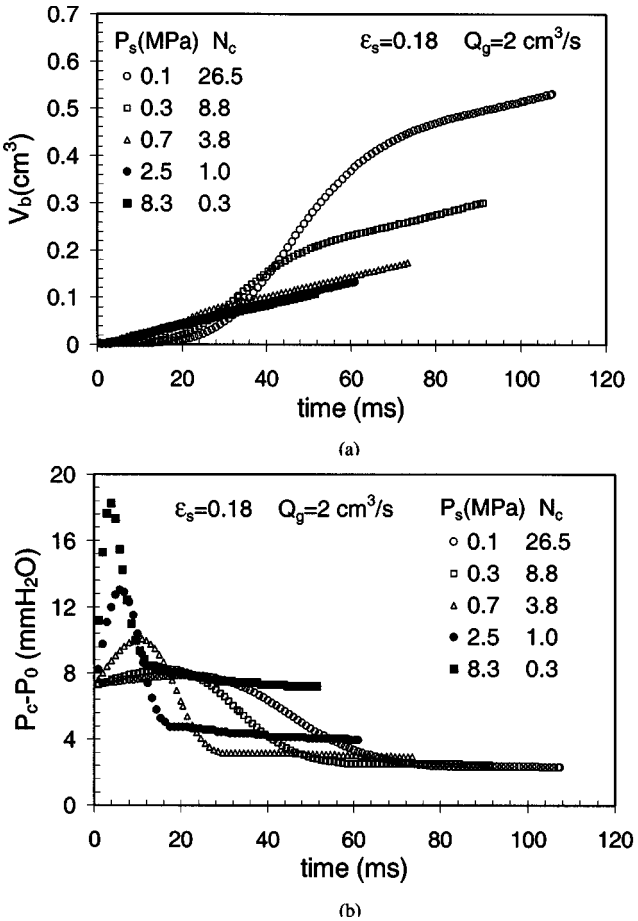

Figure 12. Pressure effect on the variation of: (a) bubble volume; (b) pressure of gas chamber with the time during the bubble-formation process.

$\epsilon_s = 0.18$, $Q_g = 2$ cm^3/s.

curves are nearly straight, which indicates that bubble formation is under constant-flow conditions. Under such conditions, an increase in pressure does not change the bubble growth rate significantly; however, it reduces the bubble growth time.

A typical variation of pressure in the gas chamber with the bubble-formation time is shown in Figure 12b. During the beginning period of bubble formation, the pressure in the gas chamber increases first due to the inflow of gas to the chamber and the inertia of liquids. Due to this increase in pressure, the bubble begins to form. When the bubble growth rate is higher than the rate at which the gas is supplied to the chamber, the amount of gas and hence the pressure in the chamber begins to decrease. As shown in Figure 12b, the pressure has a significant effect on the pressure fluctuation in the gas chamber. At ambient pressure, the pressure fluctuation in the chamber is relatively small. With an increase in pressure, the pressure fluctuation in the chamber becomes significant. It is also noted that the pressure in the gas chamber becomes constant after a certain time, which can be seen clearly at high-pressure conditions. For example, at a pressure of 2.5 MPa, the pressure in the gas chamber becomes constant after 18 ms, as shown in Figure 12b. This can be illustrated by considering the change of Q_0 with the growth time. As shown in Figure 8, when the pressure is 2.5 MPa, after 18 ms, the gas flow rate to the bubble is constant and approximately equal to the gas flow rate entering the gas chamber. This results in a constant amount of gas in the chamber, and hence a constant pressure. As shown in Figures 8 and 12, it is clear that even when the bubble formation is under constant-flow conditions, there are still fluctuations in the chamber pressure and the gas flow rate through the orifice at the start of bubble formation.

Concluding Remarks

The bubble-formation behavior from a single orifice in the liquid and liquid–liquid suspension with pressure fluctuations in the gas chamber is studied experimentally and analytically under high-pressure conditions (up to 8.3 MPa). The initial bubble size and bubbling frequency are measured using a fiber-optic probe and a high-speed video camera. An analytical model is developed to simulate the bubble formation under high pressures in the liquid–solid suspension. The model considers particle effects on the bubble motion and the pressure balance at the bubble–liquid interface. Both the experiments and the analytical model show that the initial bubble size in the suspension is generally larger than that in the liquid, and that the effect of pressure on the initial bubble size

depends on bubble-formation conditions. Under variable-flow conditions ($N_c > 1$), the initial bubble size decreases with an increase in pressure, while under constant-flow conditions ($N_c \leq 1$), the pressure effect on the initial bubble size is insignificant. The proposed model reasonably predicts the initial bubble sizes obtained in this study and those reported in the literature under high-pressure conditions. The model is also capable of predicting such instantaneous bubble-formation characteristics as the bubble growth rate, the change in gas flow rate through the orifice, and pressure fluctuations in both the gas chamber and the bubble. The model simulation indicates that during bubble formation, the pressure in the gas chamber and the gas flow rate through the orifice change significantly with time. Even for bubble formation under constant-flow conditions, there still exist pressure fluctuations in the gas chamber and gas flow-rate fluctuations through the orifice at the start of bubble formation.

Acknowledgment

This work was supported in part by National Science Foundation Grant CTS-9528380, and in part by U.S. Department of Energy Grant DEFC22-95 PC 95051, with Cooperative Agreement with Air Products and Chemicals, Inc.

Notation

A_b = surface area of bubble, m^2
C_D = drag coefficient, dimensionless
C_g = constant in Eq. 11, dimensionless
C_p = specific heat capacity of gas at constant pressure, J/(kg·K)
C_v = specific heat capacity of gas at constant volume, J/(kg·K)
D_0 = orifice diameter, m
d_b = initial bubble size, m
e = restitution coefficient, dimensionless
f = friction factor, dimensionless
f_b = bubbling frequency, Hz
F_σ = surface tension force, N
F_B = buoyancy force, N
F_{Basset} = Basset force, N
F_C = particle–bubble collision force, N
F_D = liquid drag force, N
$F_{I,g}$ = bubble inertial force, N
$F_{I,m}$ = suspension inertial force, N
F_M = gas momentum force, N
g = gravitational acceleration, m/s^2
h = liquid level in the column, m
k_0 = orifice constant, $m^3/(Pa^{0.5}\cdot s)$
L = thickness of orifice plate, m
N_c = capacitance number, dimensionless
P_0 = hydrostatic pressure at the bubble surface, Pa
P_b = pressure in the bubble, Pa
P_c = pressure in the gas chamber, Pa
$P_{c,e}$ = pressure in the gas chamber at the end of expansion stage, Pa
P_e = pressure at the gas inlet to the chamber, Pa
P_s = system pressure, Pa
Q_0 = instantaneous gas flow rate through the orifice, m^3/s
Q_g = volumetric gas flow rate entering the gas chamber, m^3/s
r_b = bubble radius, m
r_e = bubble radius at the end of expansion stage, m
Re = Reynolds number, $(\rho_l u_b d_b)/\mu_l$, dimensionless
Re_o = orifice Reynolds number, $(\rho_g u_0 D_0)/\mu_g$, dimensionless
T = temperature, K
t = time, s
t_e = time of expansion stage, s
u = rise velocity of bubble base, m/s
u_0 = instantaneous gas velocity through the orifice, m/s
u_b = rise velocity of bubble center, m/s
u_e = bubble-expansion velocity, m/s
u_g = orifice gas velocity, m/s
u_m = velocity of liquid–solid suspension, m/s
V_b = volume of bubble, m^3
V_c = volume of gas chamber, m^3
V_{neck} = volume of neck, m^3
x = distance between bubble center and orifice plate, m

Greek letters

ΔP_I = pressure change along the bubble–liquid interface due to liquid inertia, Pa
ΔP_m = pressure change along the bubble–liquid interface due to gas momentum, Pa
$\Delta P_{m,\theta}$ = pressure change at any interface element due to gas momentum, Pa
ΔP_μ = pressure change along the bubble–liquid interface due to liquid viscosity, Pa
ΔP_σ = pressure change along the bubble–liquid interface due to surface tension, Pa
δV = volume element of liquid–solid suspensions surrounding the bubble, m^3

Table 3. References Used in Figure 11 Concerning Bubble Formation Under High-Pressure Conditions

Reference	System	P_s (MPa)	V_c (cm^3)	D_0 (mm)	N_c	Q_g (cm^3/s)	Symbol in Fig. 11
Kling (1962)	N_2, Ar/H_2O	0.3 ~ 8.1	9.08	1.05	0.01 ~ 0.34	0.1 ~ 5.0	×
LaNauze and Harris (1974)	CO_2/H_2O	0.1 ~ 2.17	375	4.8	0.09 ~ 2.0	1.0 ~ 30.0	♦
Bier et al. (1978)	N_2/H_2O	0.1 ~ 2.1	1,775	1.6	4.1 ~ 84	0.1 ~ 20.0	◇
Tsuge et al. (1981)	He, N_2, Ar, CO_2/H_2O	0.1	153	1.08	16	0.1 ~ 10.0	—
Tsuge and Hibino (1983)	He, N_2, Ar, CO_2/H_2O	0.1	237	1.08	25	0.1 ~ 10.0	□
Idogawa et al. (1985)	Air/water	1.0 ~ 5.0	8.1	1.0	0.2 ~ 1.0	0.5 ~ 5.0	○
Tsuge et al. (1992)	N_2/H_2O	1.0 ~ 8.1	365	1.48	0.3 ~ 2.1	0.1 ~ 5.0	●
Wilkinson and van Dierendonck (1994)	N_2/H_2O	0.1 ~ 2.1	1775	1.6	0.4 ~ 8.7	0.1 ~ 10.0	▲
Yoo et al. (1997)	Air/glycerol/ polystyrene beads	0.1 ~ 8.0	86.2	1.18	0.1 ~ 8.1	0.1 ~ 4.0	■
Yoo et al. (1998)	CO_2, N_2/H_2O	0.1 ~ 8.0	86.2	1.48	0.06 ~ 4.9	0.1 ~ 5.0	+
Luo et al. (1998a)	N_2/NF fluid/glass beads	0.1 ~ 17.3	Const. flow	1.59	1.0	0.002 ~ 8.0	*
This work	N_2/NF fluid/glass beads	0.1 ~ 8.3	650	1.63	0.3 ~ 26.5	0.1 ~ 15.0	Δ

ϵ_l = liquid holdup, dimensionless
ϵ_s = solids concentration, dimensionless
γ = contact angle between bubble surface and orifice, rad; specific heat ratio of gas, dimensionless
μ_g = gas viscosity, Pa·s
μ_l = liquid viscosity, Pa·s
θ = angle between the radial and vertical directions of interface element, rad
ρ_g = gas density, kg/m^3
ρ_l = liquid density, kg/m^3
ρ_m = density of liquid–solid suspensions, kg/m^3
ρ_s = particle density, kg/m^3
σ = surface tension, N/m
ζ = coefficient in Eq. 2, dimensionless

Literature Cited

Bier, K., D. Gorenflo, and J. K. Karlsruhe, "Blasenbildung und Phasengrenzflache beim Dispergieren von Gasen in Flussigkeiten an Einzelnen, Gaszulaufoffnungen: Teil 2," *Warme und Stoffubertragung*, **11**, 217 (1978).

Davidson, J. F., and B. O. G. Schuler, "Bubble Formation at an Orifice in a Viscous Liquid," *Trans. Inst. Chem Eng.*, **38**, 144 (1960a).

Davidson, J. F., and B. O. G. Schuler, "Bubble Formation at an Orifice in an Inviscid Liquid," *Trans. Inst. Chem. Eng.*, **38**, 335 (1960b).

Haynes, J. B., and D. H. T. Gotham, "Heat Transfer During Bubble Formation," *Int. J. Heat Fluid Flow*, **3**, 21 (1982).

Idogawa, K., K. Ikeda, and T. Fukuda, "Formation and Flow of Gas Bubbles in a Pressurized Bubble Column with a Single Orifice or Nozzle Gas Distributor," *Chem. Eng. Commun.*, **59**, 201 (1987).

Idogawa, K., K. Ikeda, T. Fukuda, and S. Morooka, "Behavior of Bubbles in a Bubble Column under High Pressure for Air-Water System," *Kagaku Kogaku Ronbunshu*, **11**, 253 (1985).

Idogawa, K., K. Ikeda, T. Fukuda, and S. Morooka, "Behavior of Bubbles of the Air-Water System in a Column under High Pressure," *Int. Chem. Eng.*, **26**, 468 (1986).

Inga, J. R., *Scaleup and Scaledown of Slurry Reactors: A New Methodology*, PhD Thesis, Univ. of Pittsburgh, Pittsburgh, PA (1997).

Kling, G., "Uber die Dynamik der Blasenbildung beim Begasen von Flussigkeiten unter Druck," *Int. J. Heat Mass Transfer*, **5**, 211 (1962).

Kotake, S., "On the Mechanism of Nucleate Boiling," *Int. J. Heat Mass Transfer*, **9**, 711 (1966).

Kumar, R., and N. R. Kuloor, "The Formation of Bubbles and Drops," *Adv. Chem. Eng.*, **8**, 255 (1970).

Kupferberg, A., and G. J. Jameson, "Bubble Formation at a Submerged Orifice above a Gas Chamber of Finite Volume," *Trans. Inst. Chem. Eng.*, **47**, T241 (1969).

LaNauze, R. D., and I. J. Harris, "Gas Bubble Formation at Elevated System Pressures," *Trans. Inst. Chem. Eng.*, **52**, 337 (1974).

Levich, V. G., *Physicochemical Hydrodynamics*, Prentice Hall, Englewood Cliffs, NJ, p. 378 (1962).

Luo, X., D. J. Lee, R. Lau, G. Q. Yang, and L. S. Fan, "Maximum Stable Bubble Size and Gas Holdup in High-Pressure Slurry Bubble Columns," *AIChE J.*, **45**, 665 (1999).

Luo, X., G. Q. Yang, D. J. Lee, and L. S. Fan, "Single Bubble Formation in High Pressure Liquid-Solid Suspensions," *Powder Technol.*, **100**, 103 (1998a).

Luo, X., K. Tsuchiya, and L. S. Fan, "Gas Jetting and Bubble Formation in High Pressure Liquid-Solid Suspensions," *Fluidization IX*, L. S. Fan and T. M. Knowlton, eds., Engineering Foundation, New York, p. 637 (1998b).

Marmur, A., and E. Rubin, "A Theoretical Model for Bubble Formation at an Orifice Submerged in an Inviscid Liquid," *Chem. Eng. Sci.*, **31**, 453 (1976).

McAllister, R. A., P. H. McGinnis, and C. A. Plank, "Perforated-Plate Performance," *Chem. Eng. Sci.*, **9**, 25 (1958).

McCann, D. J., and R. G. H. Prince, "Bubble Formation and Weeping at a Submerged Orifice," *Chem. Eng. Sci.*, **24**, 801 (1969).

Milne-Thomson, L. M., *Theoretical Hydrodynamics*, 3rd ed., Macmillan, London (1955).

Miyahara, T., and T. Takahashi, "Bubble Volume in Single Bubbling Regime with Weeping at a Submerged Orifice," *J. Chem. Eng. Jpn.*, **17**, 597 (1984).

Pinczewski, W. V., "The Formation and Growth of Bubbles at a Submerged Orifice," *Chem. Eng. Sci.*, **36**, 405 (1981).

Poritsky, H., "The Growth or Collapse of a Spherical Bubble or Cavity in a Viscous Fluid," *Proc. U.S. First National Congress, Appl. Mech., ASME*, 313 (1952).

Ramakrishnan, S., R. Kumar, and N. R. Kuloor, "Studies in Bubble Formation—I: Bubble Formation under Constant Flow Conditions," *Chem. Eng. Sci.*, **24**, 731 (1969).

Tarmy, B., M. Chang, C. Coulaloglou, and P. Ponzi, "Hydrodynamic Characteristics of Three Phase Reactors," *Chem. Eng.*, 18 (1984).

Tsuge, H., and S. Hibino, "Bubble Formation from a Submerged Single Orifice Accompanied by Pressure Fluctuations in Gas Chamber," *J. Chem. Eng. Jpn.*, **11**, 173 (1978).

Tsuge, H., and S. Hibino, "Bubble Formation from an Orifice Submerged in Liquids," *Chem. Eng. Commun.*, **22**, 63 (1983).

Tsuge, H., Y. Nakajima, and K. Terasaka, "Behavior of Bubbles Formed from a Submerged Orifice under High System Pressure," *Chem. Eng. Sci.*, **47**, 3273 (1992).

Tsuge, H., Y. Tanaka, and S. Hibino, "Effect of the Physical Properties of Gas on the Volume of Bubble Formed from a Submerged Single Orifice," *Can. J. Chem. Eng.*, **59**, 569 (1981).

Wilkinson, P. M. *Physical Aspects and Scale-Up of High Pressure Bubble Columns*, PhD Thesis, Univ. of Groningen, Groningen, The Netherlands (1991).

Wilkinson, P. M., and L. L. van Dierendonck, "A Theoretical Model for the Influence of Gas Properties and Pressure on Single-Bubble Formation at an Orifice," *Chem. Eng. Sci.*, **49**, 1429 (1994).

Witze, C. P., V. E. Schrock, and P. L. Chambre, "Flow about a Growing Sphere in Contact with a Plane Surface," *Int. J. Heat Mass Transfer*, **11**, 1637 (1968).

Yoo, D. H., H. Tsuge, K. Terasaka, and K. Mizutani, "Behavior of Bubble Formation in Suspended Solution for an Elevated Pressure System," *Chem. Eng. Sci.*, **52**, 3701 (1997).

Yoo, D. H., K. Terasaka, and H. Tsuge, "Behavior of Bubble Formation at Elevated Pressure," *J. Chem. Eng. Jpn.*, **31**, 76 (1998).

Manuscript received Oct. 27, 1999, and revision received May 4, 2000.